J. Space Weather Space Clim. 2024, **14**, 21

https://doi.org/10.1051/swsc/2024015

JSWSC

Available online at:
www.swsc-journal.org

Topical Issue - Space Climate: Long-term effects of solar variability on the Earth's environment

RESEARCH ARTICLE OPEN ACCESS

On the uncertain intensity estimate of the 1859 Carrington storm

Jeffrey J. Love[1,*], E. Joshua Rigler[1], Hisashi Hayakawa[2,3,4], and Kalevi Mursula[5]

[1] U.S. Geological Survey, Geomagnetism Program, Geologic Hazards Science Center, Denver, CO 80225, USA
[2] Institute for Space-Earth Environmental Research, Nagoya University, Nagoya 4648601, Japan
[3] Institute for Advanced Research, Nagoya University, Nagoya 4648601, Japan
[4] RAL Space, Rutherford Appleton Laboratory, Harwell Campus, Science and Technology Facilities Council, Didcot OX11 0QX, UK
[5] Space Climate Group, Space Physics and Astronomy Research Unit, University of Oulu, PO Box 3000, 90014 Oulu, Finland

Received 28 May 2023 / Accepted 14 May 2024

Abstract – A study is made of the intensity of the Carrington magnetic storm of September 1859 as inferred from visual measurements of horizontal-component geomagnetic disturbance made at the Colaba observatory in India. Using data from modern observatories, a lognormal statistical model of storm intensity is developed, to characterize the maximum-negative value of the storm-time disturbance index (maximum *–Dst)* versus geomagnetic disturbance recorded at low-latitude observatories during magnetic storms. With this model and a recently published presentation of the Colaba data, the most likely maximum *–Dst* of the Carrington storm and its credibility interval are estimated. A related model is used to examine individual Colaba disturbance values reported for the Carrington storm. Results indicate that only about one in a million storms with maximum *–Dst* like the Carrington storm would result in local disturbance greater than that reported from Colaba. This indicates that either the Colaba data were affected by magnetospheric-ionospheric current systems in addition to the ring current, or there might be something wrong with the Colaba data. If the most extreme Colaba disturbance value is included in the analysis, then, of all hypothetical storms generating the hourly average disturbance recorded at Colaba during the Carrington storm, the median maximum *–Dst* = 964 nT, with a 68% credibility interval of [855, 1087] nT. If the most extreme Colaba disturbance value is excluded from the analysis, then the median maximum *–Dst* = 866 nT, with a 68% credibility interval of [768, 977] nT. The widths of these intervals indicate that estimates of the occurrence frequency of Carrington-class storms are very uncertain, as are related estimates of risk for modern technological systems.

Keywords: Magnetic storm / Space weather / Extreme event / Historical event / Statistical analysis

1 Introduction

The solar-geospace storm of September 1–2, 1859, commonly known as the "Carrington event", was extraordinary. Its occurrence influenced the historical development of notions of space physics and space weather (e.g., Cliver, 2006; Hudson, 2021). Today, it is widely regarded as a benchmark for extreme space weather hazards (e.g., Cliver and Dietrich, 2013; Lakhina and Tsurutani, 2018; Usoskin et al., 2023). The event started with a solar flare that was witnessed telescopically by Richard Carrington (1859) and Richard Hodgson (1859). Just 17.6 h later, ground-based magnetic observatories recorded the commencement of a magnetic storm (e.g., Cliver and Svalgaard, 2005). The short duration between the flare and the magnetic storm indicates that the Sun-Earth distance was traversed by an interplanetary coronal-mass ejection (ICME) of unusually high velocity (e.g., Cliver and Svalgaard, 2005). The resulting magnetic storm-induced interference on telegraph systems around the world (e.g., Boteler, 2006b) and spectacular aurorae in many nighttime skies (e.g., Green et al., 2006; Silverman, 2006; Hayakawa et al., 2018), some seen overhead at magnetic latitudes as low as 25.1°(e.g., Hayakawa et al., 2020a). This indicates that the Carrington magnetic storm was extremely intense. But quantification of its intensity has proven challenging because the amplitude and rapidity of geomagnetic field variation during the Carrington storm exceeded the recording capabilities of automatic analogue magnetometers then in operation at some observatories (e.g., Beggan et al., 2024).

In this context, researchers have concentrated on geomagnetic variation data reported from the Colaba observatory in Bombay (Mumbai), India (e.g., Tsurutani et al., 2003; Siscoe et al., 2006), where, at the time of the Carrington magnetic

*Corresponding author: jlove@usgs.gov

storm, geomagnetic field measurements were being made "by-eye" (Moos, 1910; Gawali et al., 2015). Although visual geomagnetic measurement methods have their limitations, they are not the same limitations suffered by automatic analogue magnetometers. Since Colaba was a low-latitude observatory, its data might be used to estimate *Dst*, a standard measure of global storm-time geomagnetic disturbance that is usually derived from data from four low-latitude observatories (Sugiura and Kamei, 1991; Karinen and Mursula, 2005). As the ring current strengthens, the horizontal component of the low-latitude geomagnetic field weakens, and *Dst* declines from a pre-storm, near-zero level to characteristically negative values (e.g., Daglis, 2006). A common measure of a magnetic storm's overall intensity is the deepest, most negative value attained by *Dst* (e.g., Gonzalez et al., 1994). But given that magnetic storms are complicated phenomena, and given that the Carrington storm is one of the most intense storms in the history of direct geomagnetic-field measurement, it is perhaps not surprising that it has been challenging to accurately estimate the Carrington storm's (global) intensity from old-fashioned disturbance data recorded (locally) at a single observatory.

In this report, we use recent observatory records of magnetic storms to develop a statistical model of storm intensity versus geomagnetic disturbance recorded locally at low-latitude observatories during magnetic storms. Using this model and a presentation by Hayakawa et al. (2022a) of the geomagnetic field data that are reported in the Colaba yearbook for 1859 (Fergusson, 1860), we estimate the most likely intensity of the Carrington storm (maximum *–Dst),* and, additionally, we obtain statistical measures of uncertainty (credibility intervals) on this intensity estimate. With a related model, we examine individual Colaba geomagnetic disturbance values reported for the Carrington storm. Important comparisons are made with Tsurutani et al. (2003), who estimated disturbance at Colaba during the Carrington storm, but with a dataset that was less complete than that of Hayakawa et al. Results inform fundamental understanding of extreme space-weather events (e.g., Hapgood, 2012), their occurrence frequency and future probability (e.g., Tsubouchi and Omura, 2007; Love, 2021), the hazards that extreme space-weather events represent for technological systems (e.g., Daglis, 2005), especially for long-line electricity transmission networks (e.g., Piccinelli and Krausmann, 2014; Ishii et al., 2021), and related risks for modern society (e.g., Baker et al., 2008; Eastwood et al., 2017; Oughton et al., 2019).

2 Local geomagnetic disturbance and Dst

Following Mursula et al. (2008), we define the ring-current index *Dst* as a discrete numerical sequence of hourly values calculated by averaging horizontal-component geomagnetic disturbance values acquired at *N* low-latitude observatories,

$$Dst(\,t_j) = \frac{1}{N}\sum_{n=1}^{N}\overline{dist}_n(t_j), \tag{1}$$

where, for each observatory *n,* hourly average disturbance is

$$\overline{dist}_n(t_j) = \frac{\overline{H}_n(t_j) - \overline{Sq}_n(t_j) - Hb_n}{cos\phi_n}. \tag{2}$$

$Sq_n(t)$ is a function representing solar-quiet variation; Hb_n is a constant baseline. $\overline{H}_n(t_j)$ is a "boxcar" average of calibrated ("absolute") sub-hourly horizontal-component magnetometer data $H_n(t_j)$ acquired within each full Universal-Time (UT) hour,

$$\overline{H}_n(t_j) = \frac{1}{M}\sum_{t_m\in[t_j]} H_n(t_m), \tag{3}$$

where the timestamp t_j for each average is the centre time of each boxcar, the bottom of each UT hour (t_j = 00:30, 01:30, etc.), and where the summation is over *M* sub-hourly samples. From 1957 until the 1980s, *Dst* was calculated using observatory hourly averages obtained from sub-hourly readings of analogue magnetograms; from the 1980s to the present time, *Dst* has been derived from digital 1-min-resolution magnetometer data. So, for example, an hourly average $\bar{H}_n(t_j)$ can be calculated by averaging M = 60 1-min $H_n(t_m)$ values, where t_m ranges from 00:00 to 00:59 UT, or from 01:00 to 01:59 UT, etc. Importantly, in equation (2), a non-stormy waveform, $\bar{S}q_n(t_j) + Hb_n$ is subtracted from each hourly average observatory hourly value, where $Sq_n(t)$ is a function that represents solar-quiet variation and Hb_n is a constant baseline. In comparison to the intense storms considered in this analysis, the peak-to-peak amplitude of solar-quiet variation is very small, ~100 nT.

Local ground-level disturbance amplitude is normalized in equation (2) under the assumption that low-latitude geomagnetic disturbance around the world can be described by a time-varying external dipolar field, with factor $1/cos\phi_n$, where ϕ_n is observatory geomagnetic latitude. Such a dipolar field would be generated by a westward-directed magnetospheric ring current (e.g., Dessler and Parker, 1959; Sckopke, 1966; Daglis, 2006). This current strengthens during the main phase of a magnetic storm, causing a decrease in the low-latitude strength of the geomagnetic field and a corresponding decrease in $Dst(t_j)$ from its near-zero quiet-time value (e.g., Loewe and Prölss, 1997), until it eventually reaches a minimum value (a maximum-negative value) that is often taken as a storm's absolute "intensity" (e.g., Gonzalez et al., 1994). Whereas a symmetric ring current would generate low-latitude geomagnetic disturbance that is symmetric across local time, other current systems, such as partial-ring, field-aligned, magnetopause, magnetotail, and ionospheric currents, introduce local-time asymmetry in disturbance (e.g., Friedrich et al., 1999; Turner et al., 2000; Ohtani et al., 2001; Asikainen et al., 2010; Saiz et al., 2021). In terms of equation (1), at any given instance in time t_j, local-time asymmetry introduces dispersion among the *N* observatory disturbance values $\overline{dist}_n(t_j)$ that contribute to the average disturbance that is $Dst(t_j)$. This dispersion, in turn, introduces inaccuracy in estimates of $Dst(t_j)$, especially if $Dst(t_j)$ is estimated from disturbance from (say) just one observatory.

Commonly, *Dst* is based on data from four standard and long-running observatories that are widely separated in longitude: Hermanus (HER), South African National Space Agency (e.g., Kotzé, 2018), Kakioka (KAK), Japan Meteorological Agency (e.g., Minamoto, 2013), and Honolulu (HON) and San Juan (SJG), U.S. Geological Survey (USGS) (e.g., Love and Finn, 2011). Some analyses of early 20th-century magnetic storms have, due to limited data availability, calculated *Dst* for alternative sets of low-latitude observatories (e.g., Love et al., 2019a; Hayakawa et al., 2020c), and some versions of *Dst*

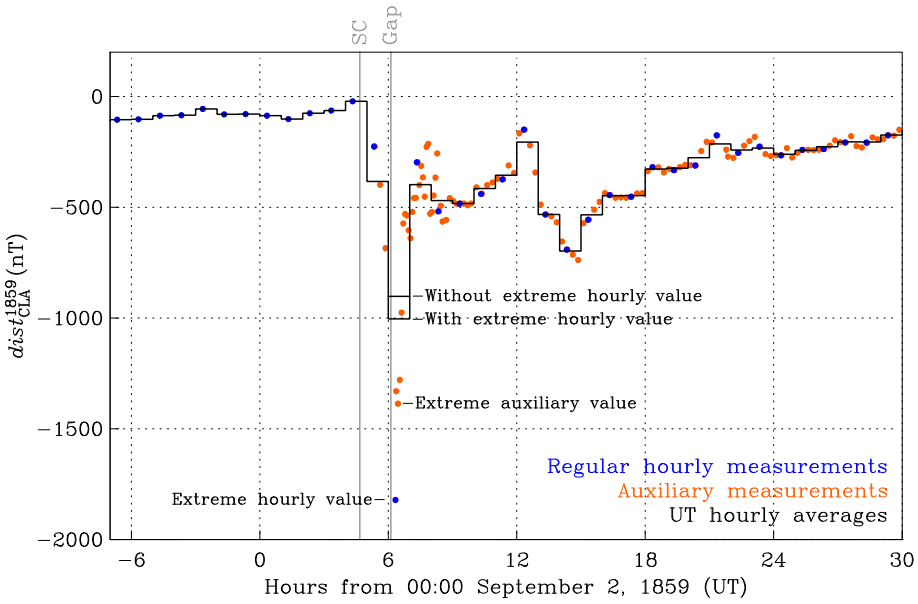

Figure 1. Time sequences of Colaba (CLA) disturbance values $dist^{1859}_{CLA}(t_j)$, equation (4), from 17:00 September 1 to 12:00 September 3, 1859, UT: regular hourly measurements (blue), auxiliary measurements (orange) made during periods of disturbance, UT-boxcar averages (black), the time of an apparent gap in the auxiliary measurements (grey). The hourly average centred on 06:30 UT is shown with and without the extreme hourly disturbance value at 06:20 UT. This figure can be compared with Hayakawa et al. (2022a). SC denotes sudden commencement; Gap denotes possible location of a data gap.

incorporate data from additional magnetic observatories (e.g., Gjerloev, 2009; Mursula et al., 2011). Since the advent of digital magnetometers, it has been possible to calculate *Dst* with 1-min resolution (e.g., Iyemori et al., 2010; Gannon and Love, 2011).

Our definition of *Dst*, as given by equation (1), is not the same as that developed for the International Geophysical Year (IGY, 1957–1958), and which is today produced by the Kyoto World Data Center (WDC). The original formulation by Sugiura (1964) was subsequently changed by Sugiura and Kamei (1991), but neither of their formulations is based on proper trigonometry (Mursula et al., 2008; Love and Gannon, 2009; Mursula et al., 2011). Unfortunately, this error affects the entire *Dst* time sequence produced by Kyoto. The importance of this issue depends on the application at hand, but Sugiura's averaging is incompatible with our analysis. For reference, in this study, we use the corrected 1-h-resolution index *Dxt* (1957-present) calculated using equation (1) by Oulu University using data from the four standard observatories (Karinen and Mursula, 2005).

3 The Colaba horizontal-component time sequence

From 1841 to 1872, variation in time t of the three components of the geomagnetic field vector, (horizontal component, declination, vertical component), was routinely monitored at the Colaba (CLA) observatory through a set of visual measurements (e.g., Gawali et al., 2015). The 1859 Colaba's yearbook records that these measurements were made every day, except Sundays and holidays (Fergusson, 1860). Routinely, and during relatively calm geomagnetic conditions, horizontal-component measurements were made at the top of each Göttingen Astronomical Time (GöT) hour, 00:00, 01:00, 02:00, etc. Additional, more frequent auxiliary measurements, what the Colaba yearbook calls "disturbance observations", were made during storms. Because both the hourly and auxiliary measurements are essentially instantaneous, they can be described as "spot" measurements. A time sequence of horizontal-component measurements $H^{1859}_{CLA}(t_j)$ (both hourly and auxiliary), each made at instances in time t_j, provides a time sequence of variation in the strength of the horizontal geomagnetic field.

In this report, we use a version of the Carrington-storm Colaba data that has recently been presented by Hayakawa et al. (2022a). They converted Colaba yearbook data from (old) English units to nanoTeslas; they adjusted for temperature-related change in instrument response; and they made the data available in computer-readable format. For this analysis, we have adjusted the data from Göttingen Astronomical Time to Universal Time; UT = GöT − 40 min + 12 h (e.g., Boteler, 2006a). For both regular-hourly and auxiliary measurements, we plot in Figure 1 the local Colaba "spot" geomagnetic disturbance time sequence, $dist^{1859}_{CLA}(t_j)$ during the Carrington storm,

$$dist^{1859}_{CLA}(t_j) = \frac{H^{1859}_{CLA}(t_j) - Sq_{CLA}(t_j) - Hb_{CLA}}{cos\phi_{CLA}}. \quad (4)$$

Here, $\Delta H^{1859}_{CLA}(t_j) = H^{1859}_{CLA}(t_j) - Hb_{CLA}$ are absolute horizontal intensities, $Sq_{CLA}(t)$ is the solar-quiet function, each as reported by Hayakawa et al. (2022a). The geomagnetic latitude at Colaba in 1859 was ϕ_{CLA} = 10.2°N.

It is useful to summarize some important details of the Colaba data that enter into our statistical analysis and our related discussion. Hourly measurements were made routinely in the days before the Carrington storm's commencement; these

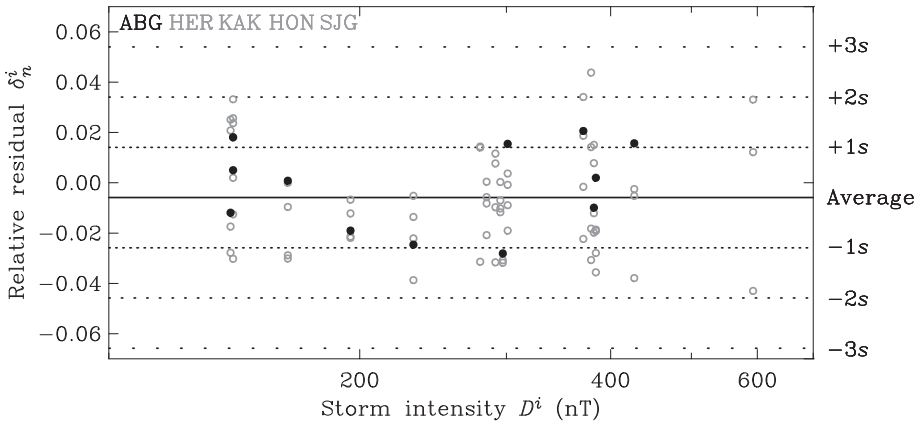

Figure 2. Relative residual differences δ_n^i, equation (6), calculated using Alibag (black, ABG), and (grey, open circle) Hermanus (HER), Kakioka (KAK), Honolulu (HON), San Juan (SJG), as a function of hourly average storm intensity D^i, equation (5), calculated using the four standard *Dst* observatories (grey) HER, KAK, HON, SJG, for the selected storms listed in Table 1 (1989–2015). Also shown: average (black solid line) of the residual differences, and standard deviation contour lines of a normal distribution (dotted lines, ±1s, etc.).

hourly measurements were also made during all subsequent phases of the Carrington storm. The most positive disturbance at Colaba has a timestamp of 04:20 UT on September 2 (17:00 GöT on September 1). This represents geomagnetic activity prior to the storm's sudden commencement – Greenwich Observatory reported that the storm commenced 20 min later, at 04:40 UT (Jones, 1955, his p. 102). After storm commencement, and during the storm's main phase, auxiliary measurements were made, initially, every 15 min. The yearbook indicates that timestamps for the auxiliary horizontal-component measurements are 2 min after "full time" (Fergusson, 1860, his p. 154), which Hayakawa et al. (2022a) interpret to mean 2 min after the reference time given in the yearbook tables (measurements of other geomagnetic components were made on different schedules relative to the reference time). With this, auxiliary horizontal-component measurements have timestamps of 05:22, 05:37, 05:52 UT (18:02, 18:17, 18:32 GöT). No auxiliary measurement is reported, when one might have been expected, for 06:07 UT (18:47 GöT); this might be regarded as a "gap" (Hayakawa et al., 2022a, their Sect. 3 and Fig. 2). The next measurement, one of those normally made on the once-per-hour schedule, has a timestamp of 06:20 UT (19:00 GöT). This value is important. It is the deepest value of the Colaba time sequence, with $dist_{\mathrm{CLA}}^{1859} = -1821$ nT. For the next two hours, auxiliary measurements were made every 5 min, with the first coming just 2 min after the regular hourly measurement, with timestamps of 06:22, 06:27, 06:32, etc. UT (19:02, 19:07, 19:12, etc. GöT). The deepest of the auxiliary disturbance value $dist_{\mathrm{CLA}}^{1859} = -1386$ nT corresponds to a measurement at 06:27 UT (19:07 GöT). Then, for an hour and a half, during what was the early part of the storm's recovery phase, measurements were made every 10 min, and they were made every 15 min for the remainder of the recovery phase.

In their analysis of the Carrington magnetic storm, Tsurutani et al. (2003) used the horizontal-component disturbance time sequence at Colaba as a proxy for a *Dst* time sequence of the Carrington magnetic storm, assuming, essentially, that $Dst(t_j) \approx dist_{\mathrm{CLA}}^{1859}(t_j)$ from Colaba. Here, it is worth emphasizing that the dataset we are using, that presented by Hayakawa et al. (2022a) from the Colaba yearbook, is not that used by Tsurutani et al. Whereas the Colaba yearbook includes auxiliary measurements made as often as every 5 min during the Carrington storm, Tsurutani et al. only report that auxiliary measurements were made every 15 min. Whereas Hayakawa et al. obtained a solar-quiet $Sq_{\mathrm{CLA}}(t)$ waveform and baseline $\mathrm{Hb}_{\mathrm{CLA}}$ using methods akin to those used in the standard estimation of *Dst* (Sugiura, 1964; Sugiura and Kamei, 1991), by averaging several quiet days of Colaba data from the month of August 1859, Tsurutani et al. used data from the day before the commencement of the Carrington storm to estimate a constant baseline without accommodation of solar-quiet variation. But, as noted by Hayakawa et al., the August 29 storm was still affecting the local horizontal-component variation prior to the occurrence of the September 2 storm, and this appears to have affected the baseline estimate of Tsurutani et al. As a result, the deepest disturbance value we quote here, $dist_{\mathrm{CLA}}^{1859} = -1821$ nT, is deeper than the –1600 nT (–1626 nT with latitude factor) value of Tsurutani et al.

4 Colaba hourly values and their accuracy

Tsurutani et al. (2003) used their estimate of the deepest disturbance value of –1600 nT (–1626 nT with latitude factor) at 06:20 UT as a spot measure of the Carrington storm's deepest *Dst* value. Subsequently, Siscoe et al. (2006) noted that, consistent with our discussion in Section 2, *Dst* is traditionally a 1-h resolution index, with boxcar averaging performed over subhourly data within each UT hour. They suggested that, in contrast to Tsurutani et al., if the Colaba disturbance data are to be used to estimate the intensity of the Carrington storm, then those data should be averaged in each UT-hour so that comparisons can be made with the traditional definition of the *Dst* index.

In Figure 1, we plot the UT-hour averages of the Colaba disturbance data. The deepest average is for the 06:00–07:00 UT window, with a centered timestamp of 06:30 on September 2. This window encompasses the extreme disturbance value at 06:20 UT and eight auxiliary measurements at 06:22, 06:27, 06:32, …, 06:57 UT. In averaging these data, we consider two scenarios, one with and the other without the extreme

Table 1. Hourly average storm intensities D^i, equation (5), calculated using the four standard observatories, Hermanus (HER), Kakioka (KAK), Honolulu (HON), and San Juan (SJG); and relative residual differences δ_n^i, equation (6), for Alibag (ABG), HER, KAK, HON, SJG, each for selected storms (1989–2015). Month (Mn), Day (Dy), Hour (Hr, UT). Data are shown in Figure 2. No δ_n^i values are listed if no observatory data are available.

Year	Mn	Dy	Hr	D^i (nT)	δ^i_{ABG}	δ^i_{HER}	δ^i_{KAK}	δ^i_{HON}	δ^i_{SJG}
1989	03	14	01	593		–0.0430	+0.0331	+0.0122	
1991	11	09	01	379		–0.0307	+0.0142	–0.0182	+0.0438
1991	03	25	00	295		–0.0070	+0.0003	–0.0117	–0.0102
1990	04	10	15	291		+0.0077	+0.0116	–0.0097	–0.0316
1992	05	10	14	284		–0.0057	–0.0208	–0.0082	+0.0004
1991	10	29	08	279		+0.0144	–0.0314	+0.0140	
2003	11	20	20	427	+0.0157	–0.0379	–0.0052		–0.0025
2003	10	30	22	384	+0.0020	–0.0356	–0.0279	–0.0192	–0.0186
2001	03	31	08	382	–0.0099	+0.0151	–0.0198	+0.0078	–0.0121
2004	11	08	06	371	+0.0206	–0.0016	+0.0187	+0.0341	–0.0223
2000	07	16	00	301	+0.0155	+0.0037	–0.0089	–0.0190	–0.0008
2000	04	06	22	297	–0.0281	–0.0308	–0.0318		
2015	03	17	22	232	–0.0246	–0.0136	–0.0387	–0.0221	–0.0052
2015	06	23	04	195	–0.0190	–0.0067	–0.0122	–0.0219	–0.0214
2015	12	20	22	164	+0.0008	–0.0096	–0.0288	–0.0301	+0.0000
2012	03	09	08	141	+0.0050	+0.0257	+0.0332	+0.0180	–0.0302
2012	07	15	16	141	+0.0181	+0.0020	+0.0237		–0.0125
2011	10	25	01	140	–0.0119	–0.0278	+0.0208	–0.0174	+0.0251

disturbance value at 06:20 UT. This leads to $\overline{dist}^{1859}_{CLA} = -1004$ and –902 nT for the 06:30 UT Colaba hourly average disturbance; refer to Figure 1. The range of these values encompasses the deepest (running-average) values of Hayakawa et al. (2022a), $\overline{dist}^{1859}_{CLA} = -979$ and –918 nT, again, depending on whether or not the extreme disturbance value at 06:20 UT is used.

Next, we check the accuracy of the UT-boxcar averages of the sparse and non-uniformly distributed Colaba disturbance data (for background, Love, 2009; Love et al., 2010). How representative are such hourly averages compared to, say, averages of data acquired densely and uniformly over a given hour? To answer this question, we examine hourly averages of modern observatory horizontal-component data acquired during extremely intense magnetic storms. We define the intensity of a storm i as the maximum $-Dst$ value realized over the storm's course

$$D^i = \max_{t^i_j \in [t^i_s, t^i_e]} \left(-Dst\left(t^i_j\right) \right), \tag{5}$$

Where t^i_s and t^i_e are the start and end times of each storm. We identify 18 intense storms, the six most intense storms in the Oulu *Dxt* time sequence for each of solar cycles 22, 23, and 24, years 1989–2015; intensities for these storms are listed in Table 1. Then, for each of these storms, we obtain digital 1-min-resolution geomagnetic horizontal-component time sequences from the Alibag (ABG) observatory in India and the four *Dst* observatories (HER, KAK, HON, SJG). Note, to avoid interference from the electrification of Bombay (Mumbai) trams, Colaba geomagnetic monitoring operations were transferred to nearby Alibag in 1904 (e.g., Gawali et al., 2015). For the UT-hour of the maximum intensity of each storm t^i and for each observatory n, we calculate the UT-boxcar hourly average of 60 1-min, ${}_{60}\overline{H}_n(t^i)$ values. Additionally, we subsample the 1-min geomagnetic time sequences in such a way as to mimic the sampling contributing to the most extreme hourly disturbance at 06:30 UT: like the regular hourly sampling at Colaba, we use for averaging horizontal-component values at the 20th minute of each UT hour, and, also, like the auxiliary sampling at Coloaba, we use values at minutes 22, 27, 32, …, 57. For the UT-hour of the maximum intensity of each storm t^i and for each observatory n, we calculate their average ${}_{C}\overline{H}_n(t^i)$. From these hourly averages, we form the relative residual differences

$$\delta^i_n = \frac{{}_{C}\overline{H}_n(t^i) - {}_{60}\overline{H}_n(t^i)}{D^i \cdot cos\phi_n}. \tag{6}$$

These values are also listed in Table 1.

In Figure 2, we plot the relative residuals δ^i_n from Table 1 as a function of storm intensity D^i. Importantly, the average of the relative residuals is very small, 0.0141, or about one per cent. This means that the ${}_{C}\overline{H}^i_n$ averages are close to being unbiased estimates of the complete averages ${}_{60}\overline{H}^i_n$. The standard deviation, s, of the relative residuals is also small, 0.0200, or just two per cent. This means that the ${}_{C}\overline{H}^i_n$ averages are, for our purposes, accurate estimates of the complete averages ${}_{60}\overline{H}^i_n$. We also note that the relative residuals do not show a significant trend across D^i. In light of these observations, we have confidence in using UT-hourly averages of the Colaba observations.

5 Estimating Carrington storm intensity with error bars

In this section, we investigate the accuracy of estimates of Carrington-storm intensity based on disturbance data from the Colaba observatory. To that end, we examine the relationship between maximum –*Dst* realized during extremely intense magnetic storms and hourly averages of geomagnetic disturbance

Table 2. Hourly average storm intensities D^i, equation (5), calculated using the four standard observatories, Hermanus (HER), Kakioka (KAK), Honolulu (HON), and San Juan (SJG); and hourly average local intensities $\overline{d}^i_n$, equation (7), calculated using Alibag (ABG) and HER, KAK, HON, SJG, each for selected storms (1957–2015). Month (Mn), Day (Dy), Hour (Hr, UT). Data in local-noon sector (09:00–14:59) are listed in bold. Data are shown in Figures 3 and 4.

Year	Mn	Dy	Hr	D^i (nT)	Mn	Dy	Hr	$\overline{d}^i_{\mathrm{ABG}}$ (nT)	Mn	Dy	Hr	$\overline{d}^i_{\mathrm{HER}}$ (nT)	Mn	Dy	Hr	$\overline{d}^i_{\mathrm{KAK}}$ (nT)	Mn	Dy	Hr	$\overline{d}^i_{\mathrm{HON}}$ (nT)	Mn	Dy	Hr	$\overline{d}^i_{\mathrm{SJG}}$ (nT)
1959	07	15	19	**429**	07	15	20	390	07	15	19	554	07	15	19	403	07	15	19	339	07	15	19	**422**
1958	02	11	10	**424**	02	11	11	456	02	11	10	**382**	02	11	11	475	02	11	09	473	02	11	10	402
1957	09	13	10	**422**	09	13	10	**527**	09	13	09	**394**	09	13	10	495	09	13	10	495	09	13	11	322
1967	05	26	04	**386**	05	26	04	379	05	26	06	341	05	26	03	**429**	05	26	03	451	05	26	01	429
1970	03	08	22	**283**					03	08	22	310	03	08	23	252	03	09	00	**266**				
1969	03	24	01	**227**	03	24	10	**272**	03	24	10	**225**	03	24	10	292	03	24	10	252	03	24	01	299
1982	07	14	03	**318**	07	14	01	291	07	14	01	346	07	14	00	**430**	07	14	03	404	07	14	03	325
1982	09	06	17	**286**	09	06	11	388	09	06	17	362	09	06	11	343	09	06	12	328	09	06	18	**297**
1981	04	13	06	**279**	04	13	06	**252**	04	13	06	261	04	13	06	285					04	13	05	314
1989	03	14	01	**593**					03	14	01	646	03	14	00	**655**	03	14	00	**588**				
1991	11	09	01	**379**	11	09	01	291	11	09	01	339	11	09	02	**354**	11	09	02	401	11	09	00	496
1991	03	25	00	**295**	03	25	00	265	03	25	00	300	03	25	02	**290**	03	25	02	331	03	25	01	339
2003	11	20	20	**427**	11	20	19	644	11	20	21	420	11	20	19	469					11	20	19	**556**
2003	10	30	22	**384**	10	30	22	400	10	30	23	358	10	30	23	326	10	30	22	**374**	10	30	22	508
2001	03	31	08	**382**	03	31	08	**378**	03	31	18	348	03	31	08	412	03	31	08	473	03	31	08	326
2015	03	17	22	**232**	03	17	16	273	03	17	19	245	03	17	22	187	03	17	23	**250**	03	17	23	302
2015	06	23	04	**195**	06	23	04	226	06	22	20	215	06	23	04	**227**	06	23	04	265	06	23	03	153
2015	12	20	22	**164**	12	20	17	185	12	20	18	180	12	21	00	**149**	12	21	02	171	12	20	22	224

Table 3. Kolmogorov-Smirnov p-values calculated for pairs of hourly average observatory intensities $\overline{d}^i_n$, equation (7), for Alibag (ABG), Hermanus (HER), Kakioka (KAK), Honolulu (HON), and San Juan (SJG), for the i storms listed in Table 2 (1957–2015).

	HER	KAK	HON	SJG
ABG	0.2182	0.2685	0.2645	0.0994
SJG	0.2182	0.2182	0.2518	
HON	0.2421	0.4255		
KAK	0.2182			

recorded at several low-latitude observatories during those storms. We identify 18 intense magnetic storms, the three most intense storms in the Oulu *Dxt* time sequence for each of solar cycles 19 through 24, years 1957–2015. Then, for the same 18 storms, we estimate hourly average horizontal-component disturbance time sequences $\overline{dist}_n\left(t^i_j\right)$ for five observatories, Alibag and the four standard *Dst* observatories. For each storm i and each observatory n, we identify the maximum-negative geomagnetic disturbance value,

$$\overline{d}^i_n = \max_{t^i_j \in \left[t^i_s, t^i_e\right]} \left(-\overline{dist}_n\left(t^i_j\right)\right), \tag{7}$$

which we call a "local hourly average intensity". In Table 2, we list the storm intensities D^i and local hourly average intensities $\overline{d}^i_n$ values for the 18 chosen storms. A few observations are worth making. The most intense storm (1957–2015) is that of March 1989 (e.g., Allen et al., 1989; Boteler, 2019); D^{1989} = 593 nT was attained at 01:30 UT on March 14. For that storm, local hourly average intensity values $\overline{d}^{1989}_n$ are only available for three (Hermanus, Kakioka, Honolulu) of the five observatories we consider because of data gaps at Alibag and San Juan. For Hermanus, the local intensity value $\overline{d}^{1989}_{HER}$ occurred at the same time as D^{1989} (01:30 UT), whereas the $\overline{d}^{1989}_n$ value for each of Kakioka and Honolulu occurred one hour earlier (00:30, March 14).

An important issue to consider is the inconsistency of the local hourly average intensities listed in Table 2. Can we tell if differences between $\overline{d}^i_n$ from pairs of observatories are statistically significant? We use a two-sample Kolmogorov-Smirnov algorithm (e.g., Press et al., 1992, Chapter 14.3; Bohm and Zech, 2010, Chapter 10.3.5) to calculate the probability (p-value) that local hourly average intensities from pairs of observatories could be independent statistical realizations from the same distribution. However, we recognize that the local intensities in each column of Table 2 are correlated – they correspond to the same 18 storms. Because tests of statistical significance assume that data are independent, this correlation in Table 2 must be removed to obtain meaningful probability estimates (e.g., von Storch, 1995; Wilks, 2006, Chapter 5). We remove it by bootstrap resampling (e.g., Efron and Tibshirani, 1994; Olea and Pawlowsky-Glahn, 2009). For a given pair of observatories, we make many random samplings with replacement of the local hourly average intensities, in each case, calculating a Kolmogorov-Smirnov p-value for pairs of observatories; we keep the median p-value of the resamplings as a suitable estimate of significance. These probabilities are listed in Table 3. We note, for example, that the probability that $\overline{d}^i_{\mathrm{KAK}}$ and $\overline{d}^i_{\mathrm{HON}}$ could be realized from two independent statistical samplings of the same distribution is 0.4255. This is a relatively

high probability, too high to confidently reject the hypothesis that the Kakioka and Honolulu local hourly average intensities are samples of the same distribution. On the other hand, the p-value for the discrepancy between $\overline{d}^i_{\mathrm{ABG}}$ and $\overline{d}^i_{\mathrm{SJG}}$ is lower at 0.0994, but even this is too high to confidently reject the hypothesis that the Alibag and San Juan local hourly average intensities are samples of the same distribution. More generally, the Kolmogorov-Smirnov p-values listed in Table 3 do not allow confident rejection of the hypothesis that the local hourly average intensities from one observatory and another observatory are samples of the same distribution. We return to the subject of Kolmogorov-Smirnov testing below when we examine the statistical consistency of datasets and models fitted to those datasets.

In seeking a plausible statistical estimate of the intensity of the Carrington storm based on local intensity data from Colaba, we need a model motivated by general physical principles. In this regard, we recognize that, fundamentally, space weather is the integrated result of the history of nonlinear (multiplicative) interaction of magnetospheric-ionospheric processes operating under external forcing by the solar wind (e.g., Vassiliadis et al., 2000; Boaghe et al., 2001). We assume, therefore, that D^i and $\overline{d}^i_n$ arise from a stochastic process involving the multiplication of many underlying random variables, and per the discussion in the Appendix, this would plausibly result in data that are lognormally distributed. Recognizing that if a population of random variables is lognormally distributed, then the logarithms of those variables will be normally distributed, we hypothesize that a given logarithmic local intensity $\ln \overline{d}^i_n$ can be generated by storms with a statistical distribution of logarithmic intensities $\ln D$,

$$g\left(\ln D^i \mid \ln \overline{d}^i_n, \ln\alpha,\, \sigma\right) = \frac{1}{\sigma\sqrt{2\pi}} \exp\left[-\frac{\left(\ln D^i - \ln \overline{d}^i_n - \ln\alpha\right)^2}{2\sigma^2}\right]. \tag{8}$$

The mean of $\ln D^i$ is the parameter $\ln \overline{d}^i_n + \ln\alpha = \ln\left(\overline{d}^i_n \cdot \alpha\right)$, the standard deviation of $\ln D^i$ is the parameter σ, and α is a bias parameter. For the storm intensities and local intensities listed in Table 2 (1957–2015), we obtain the parameters $\{\ln\alpha, \sigma\}$ in the probability density function (8) by the method of maximum likelihood (e.g., Roe, 2001; Bohm and Zech, 2010). The joint probability density of the intensity data, given the model parameters, is the likelihood function

$$\mathfrak{L}(\ln\alpha,\, \sigma) = \prod_{i,n=1}^{I,N} g\left(\ln D^i | \ln \overline{d}^i_n,\, \ln\alpha,\, \sigma\right), \tag{9}$$

where multiplication is over the I storms contributing to the likelihood and the N observatories, with appropriate accommodation for missing values. The model parameters giving the maximum (the mode) of $\mathfrak{L}$ is the most likely solution,

$$\ln\alpha = \frac{1}{I\cdot N}\sum_{i,n=1}^{I,N}\left(\ln D^i - \ln \overline{d}^i_n\right), \tag{10}$$

$$\sigma^2 = \frac{1}{I\cdot N}\sum_{i,n=1}^{I,N}\left(\ln D^i - \ln \overline{d}^i_n - \ln\alpha\right)^2. \tag{11}$$

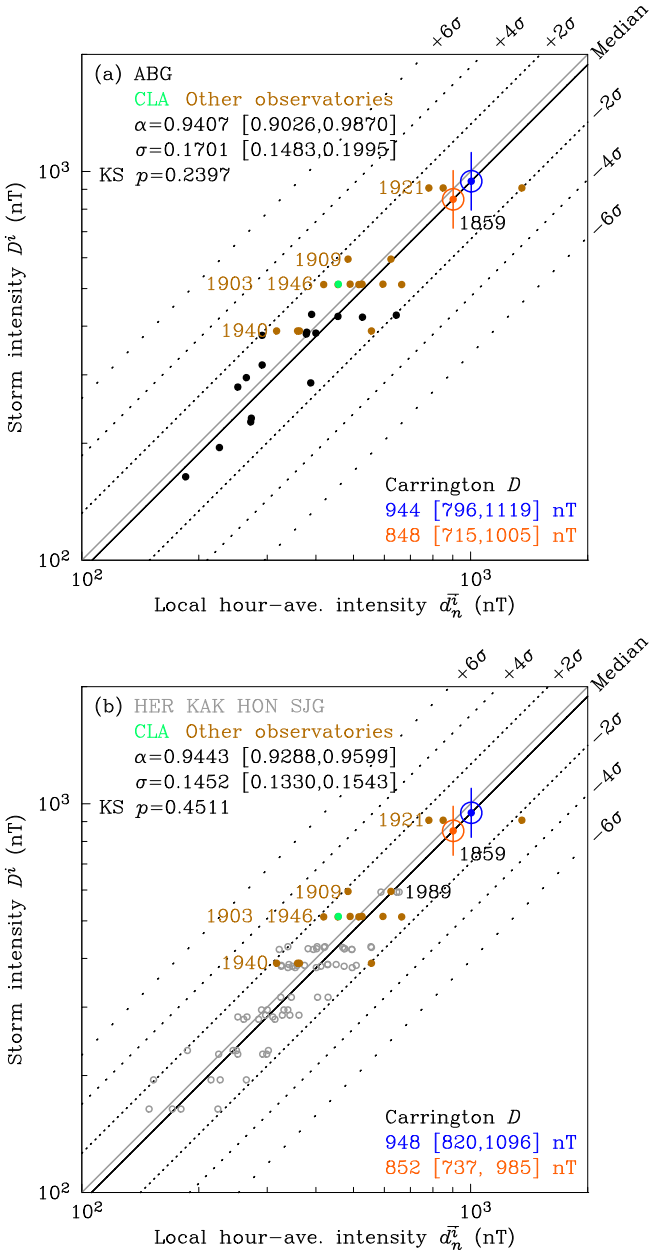

Figure 3. Contour lines of the (log)normal density function $g(\ln D^i|\ln \overline{d}^i_n,\, \ln\alpha,\, \sigma)$, equation (8): median (black solid line) and (black dotted lines) $\pm 2\sigma$, etc. intervals (dotted lines); intensities D^i and $\overline{d}^i_n$ from Table 2 (1957–2015): (a) Alibag (black, ABG) and (b) the four standard *Dst* observatories (grey, open circles), Hermanus (HER), Kakioka (KAK), Honolulu (HON), San Juan (SJG). Also shown: data from Table 4 (brown, green) for five other superstorms (1903, 1909, 1921, 1940, 1946). In each of (a, b) estimates of Carrington-storm D^{1859} are shown for Colaba $\overline{d}^{1859}_{CLA}$ with (blue) and without (orange) the extreme disturbance value at 06:20 UT. 68% ($\pm 1\sigma$) credibility intervals in brackets. Bootstrap Kolmogorov-Smirnov probability, KS p.

In Figure 3, we plot the (log)normal density functions $g(\ln D^i|\ln \overline{d}^i_n,\, \ln\alpha,\, \sigma)$ and data from Table 2 separately (a) for data from Alibag and (b) for data from the four standard *Dst* observatories,

Table 4. Hourly average superstorm intensities D^i, equation (5), calculated for observatory (Obs) hourly average intensities $\overline{d}^i_n$, equation (7), for selected storms. Month (Mn), Day (Dy), Apia (API), Cape Town (CTO), Colaba (CLA), Coimbra (COI), Cuajimalpa (CUA), Hermanus (HER), Honolulu (HON), Kakioka (KAK), Mauritius (MRI), San Fernando (SFS), San Juan (SJG), Vieques (VQS), Watheroo (WAT), and Zi-Ka-Wei (ZKW). Data in local-noon sector (09:00–14:59) are listed in bold. Data are shown in Figures 3 and 4.

Year	Mn	Dy	D^i (nT)	Obs	$\overline{d}^i_n$ (nT)	Obs	$\overline{d}^i_n$ (nT)	Obs	$\overline{d}^i_n$ (nT)	Obs	$\overline{d}^i_n$ (nT)	Source
1903	10	31	**513**	COI	**526**	CLA	457	ZKW	595	CUA	490	Hayakawa et al. (2020c)
1909	09	25	595	SFS	624	MRI	–	API	484	VQS	–	Love et al. (2019b)
1921	05	15	**907**	SFS	–	WAT	**1335**	API	850	VSS	781	Love et al. (2019a)
1940	03	24	**398**	CTO	359	KAK	363	HON	**317**	VSS	556	Hayakawa et al. (2022b)
1946	03	28	**512**	HER	**419**	WAT	665	HON	456	SJG	**516**	Hayakawa et al. (2020b)

Hermanus, Kakioka, Honolulu, and San Juan. We see, immediately, that the model based on Alibag data is similar to that based on data from the *Dst* observatories. In both cases, a log-normal model characterizes the intensity data across wide ranges in both ln $\overline{d}^i_n$ and ln D^i – the relationship between these two variables appears to be scale-invariant (see Appendix). For comparison, in Figure 3 we also plot the intensity data given in Table 4 for five superstorms, those of October 1903 (Hayakawa et al., 2020c), September 1909 (Hayakawa et al., 2019; Love et al., 2019b), May 1921 (Hapgood, 2019; Love et al., 2019a), March 1940 (Hayakawa et al., 2022b), and March 1946 (Hayakawa et al., 2020b); these data, which are not used in fitting the model, provide validation of the model (and its underlying hypotheses) for the most extreme values of $\overline{d}^i_n$ and D^i. As above, we perform Kolmogorov-Smirnov tests, but this time we use a one-sample algorithm to calculate the probability that the local intensity data are statistical realizations from the fitted models. We recognize that it is not meaningful to test for significance between a dataset and a model that has been fitted to those data – they are not statistically independent. We can, however, examine statistical significance under bootstrap resampling (e.g., Steinskog et al., 2007; Clauset et al., 2009, their Section 3.4; Corral and González, 2019, their Section 3.2). Bearing that in mind, we treat each of the two (log)normal models (a,b) shown in Figure 3 as hypothetical: we make multiple random samplings of the intensity data with replacement, and with each resampling, we calculate a Kolmogorov-Smirnov *p*-value against the model; median *p*-values from multiple resamplings are suitably unbiased estimates of significance. These bootstrap *p*-values are listed in Figure 3; these are not small enough to motivate rejection of the hypothesis that the intensity data are realized from a (log)normal processes.

Importantly, we can use the models in Figure 3 to estimate the Carrington storm's intensity D^{1859} and the corresponding accuracy of D^{1859} given the local hourly average intensity $\overline{d}^{1859}_{\mathrm{CLA}}$ from Colaba. We recall from Section 4 our pair of estimates of local hourly average intensity during the Carrington storm, $\overline{d}^{1859}_{\mathrm{CLA}} = 1004$ and 902 nT, depending on whether or not the extreme disturbance value at 06:20 UT is included in the averaging. In Figure 3(a), where the model is fitted to the Alibag intensity data, the bias parameter is $\alpha = 0.9407$, and the dispersion parameter is $\sigma = 0.1701$. With this, we obtain $D^{1859} = \alpha \cdot \overline{d}^{1859}_{\mathrm{CLA}} = 944$ nT (blue) as the median intensity of all hypothetical storms generating a local hourly average intensity of $\overline{d}^{1859}_{\mathrm{CLA}} = 1004$ nT. A 68% credibility interval for such a storm intensity is $[D^{1859} \cdot \mathrm{e}^{-\sigma}, D^{1859} \cdot \mathrm{e}^{+\sigma}] = [796,1119]$ nT – for a width of 323 nT. On the other hand, $D^{1859} = 848$ nT (orange) for the median intensity of all hypothetical storms generating a local hourly average intensity of $\overline{d}^{1859}_{\mathrm{CLA}} = 902$ nT. A 68% credibility interval for such a storm intensity is [715,1005] nT – for a width of 290 nT. The two intervals, one for inclusion of the extreme value and one for its exclusion, are overlapping. We might, therefore, infer that the difference between the estimated Carrington storm intensities is insignificant. In Figure 3(b), for data from the *Dst* observatories, the model is very similar to that shown in Figure 3(a), for the Alibag data – the confidence intervals for α and σ are overlapping. This indicates that the models are not significantly affected by correlations between the local hourly average intensities $\overline{d}^i_n$ from the various *Dst* observatories. This observation reinforces the confidence we have in our estimates of the intensity of the Carrington storm inferred from data from Colaba.

Siscoe et al. (2006, their Section 2) called attention to the important fact that, in terms of local time, the Colaba observatory was just about ideally situated for providing disturbance data that approximate *Dst*, because local disturbance tends to be greater (less) than *Dst* at local dusk (local dawn) and approximately equal to *Dst* at local noon and midnight (Chapman and Bartels, 1962, their Chapter 9.3; Love and Gannon, 2009, their Section 6.2). This indicates that at least part of the dispersion in D^i seen in Figure 3 is due to data sampling across dawn-dusk asymmetry. Therefore, for similarity with Colaba measurements made around local noon, we now restrict ourselves to the intensities in Table 2 realized in the local-time sector 09:00 to 14:59. We also note the consistency seen in Figure 3(a) and (b), and so we treat the local noon-sector data from the *Dst* observatories and Alibag together and obtain a (log)normal model by maximum likelihood. In Figure 4, we plot corresponding results. The bias factor, $\alpha = 0.9603$, is a bit closer to 1.0000, than for the results in Figure 3, meaning a smaller average difference between storm intensity D^i and local hourly average intensity $\overline{d}^i_n$. The standard deviation, $\sigma = 0.1204$, is smaller than for the results in Figure 3, meaning more accurate estimates of D^i for a given $\overline{d}^i_n$. Including the extreme disturbance value leads to a local hourly average intensity of $\overline{d}^{1859}_{\mathrm{CLA}} = 1004$. From that, we obtain a median storm intensity of $\mathrm{D}^{1859} = \alpha \cdot \overline{d}^{1859}_{\mathrm{CLA}} = 964$ nT and a 68% credibility interval of $[D^{1859} \cdot \mathrm{e}^{-\sigma}, D^{1859} \cdot \mathrm{e}^{+\sigma}] = [855, 1087]$ nT – for a width of 232 nT. We note that the maximum (hourly average) – *Dst* estimate of ~850 nT given by Siscoe et al. is just outside and lower than our 68% credibility interval; on the other hand, the maximum (hourly average) –*Dst* estimate of ~1050 nT (Gonzalez et al., 2011) is within our 68% credibility interval. Excluding the extreme value at 06:20 UT leads to a local hourly average intensity of $\overline{d}^{1859}_{\mathrm{CLA}} = 902$ nT. From this, we obtain a median storm intensity $D^{1859} = 866$ nT and a

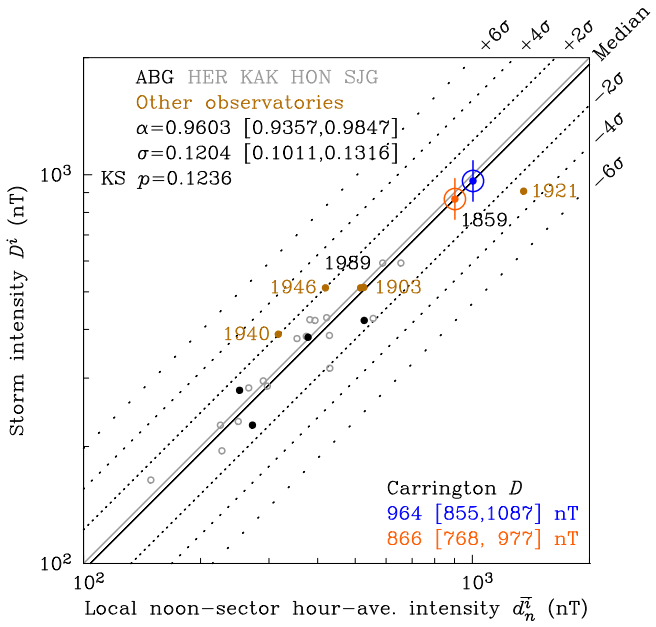

Figure 4. Same as Figure 3, except that, to mimic sampling performed at Colaba during the Carrington storm, intensities D^i and $\bar{d}_n^i$ are restricted to the local noon sector 09:00 to 14:59, bold values in Table 2.

68% credibility interval of [768, 977] nT – for a width of 209 nT. These results represent our best estimates of the Carrington storm's intensity and its statistical uncertainty.

6 Rarity of local intensity values

The spot disturbance value $dist_{\mathrm{CLA}}^{1859} = -1821$ nT at 06:20 UT on September 2, 1859, is, among all the hourly and auxiliary values from Colaba, the most extreme. To put this into perspective, we examine modern 1-min-resolution observatory measurements recording 18 intense storms, years 1989–2015 (cycles 22–24) – the same 18 storms used in Section 4. For each storm i, we obtain its intensity D^i. For each storm i and each observatory n, we estimate local disturbance sequences by using an algorithm specifically designed for separating 1-min-resolution $Sq_n^i(t_j) + Hb_n^i$ from an observatory horizontal intensity sequence (Rigler, 2017); we apply a latitude factor as per equation (4). Then, per Section 4, to mimic the sampling schedule at Colaba, for each UT hour, we use for analysis the disturbance value at the 20th UT-minute of each hour, and like the Colaba auxiliary values, we use disturbance values at UT-minutes 2, 7, 12, …, 57. For each storm i and each observatory n, we denote these Colaba-like disturbance values as $dist_n({}_C t_j^i)$. From these samples, we identify the maximum negative geomagnetic disturbance value,

$$ {}_C d_n^i = \max_{{}_C t_j^i \in [t_s^i, t_e^i]} \left(-dist_n\left({}_C t_j^i \right) \right); \tag{12} $$

compare with equation (7). Finally, we restrict ourselves to local intensities realized in the local-noon sector. Individual values are listed in Table 5.

Next, we examine a model in which storms with a given logarithmic intensity $\ln D^i$ will give rise to local logarithmic intensities $\ln {}_C d_n^i$ that are normally distributed,

$$ g\left(\ln {}_C d_n^i \,|\, \ln D^i,\, \ln \alpha,\, \sigma\right) = \frac{1}{\sigma\sqrt{2\pi}} \exp\left[-\frac{\left(\ln {}_C d_n^i - \ln D^i - \ln \alpha\right)^2}{2\sigma^2} \right]. \tag{13} $$

Here, the mean of $\ln {}_C d_n^i$ is the parameter $\ln D + \ln \alpha = \ln(D^i \cdot \alpha)$, the standard deviation of $\ln {}_C d_n^i$ is the parameter σ, and α is, again, a bias parameter. As per the Appendix, equation (13) can be recognized as the Bayesian dual of equation (8) and vice versa. Combining data from Alibag with those from the standard *Dst* observatories, we obtain the (log)normal model parameters $\{\ln \alpha, \sigma\}$ in the probability density function (13) by the method of maximum likelihood. We plot results in Figure 5. The bootstrap-resampled Kolmogorov-Smirnov probability, developed per Section 5, is too high to reject the (log)normal hypothesis. For comparison, in Figure 5, we plot the extreme hourly intensity, $d_{CLA}^{1859} = 1821$ nT, together with our corresponding estimate of the Carrington storm's intensity, $D^{1859} = 964$ nT, with the inclusion of the extreme disturbance value at 06:20 UT. We also plot the extreme auxiliary intensity, $d_{CLA}^{1859} = 1386$ nT, corresponding to a measurement at 06:27 UT, together with our corresponding estimate of the Carrington storm's intensity, $D^{1859} = 866$ nT, with exclusion of the extreme disturbance value at 06:20 UT. The extreme hourly intensity value is close to 5.4σ from the median, whereas the extreme auxiliary intensity value is more than 4.0σ from the median.

From the complementary cumulative, we obtain the exceedance probability

$$ \begin{aligned} G\left(\ln {}_C d_n^i \,|\, \ln D^i,\, \ln \alpha,\, \sigma \right) &= \int_{\ln {}_C d_n^i}^{+\infty} g(\xi \,|\, \ln D^i,\, \ln \alpha,\, \sigma) d\xi \\ &= \frac{1}{2}\left[1 - \mathrm{erf}\left(\frac{\ln {}_C d_n^i - \ln D^i - \ln \alpha}{\sigma\sqrt{2}} \right) \right]. \end{aligned} \tag{14} $$

From this, we can estimate the probability that a storm with intensity $D^{1859} = 964$ nT would give rise to an hourly local intensity greater than $d_{\mathrm{CLA}}^{1859} = 1821$ nT. The probability is very low, $G < 10^{-6}$, or $1/G > 10^6$. In other words, under the (log) normal hypothesis, only one out of about a million storms with intensities like the Carrington storm would result in a local noon-sector hourly intensity greater than that reported from Colaba. Note, also, that the extreme auxiliary intensity at 06:27 UT would be a very unusual realization, $G = 0.000027$, for a storm with an intensity like that of the Carrington storm. These probabilities are so small they strain credulity.

At least two explanations need to be considered. First, it is possible that the geomagnetic disturbance recorded at Colaba during the Carrington storm was, in addition to being affected by the ring current, unusually affected by other current systems in the magnetosphere and ionosphere (e.g., Cliver and Svalgaard, 2005). Phenomenological analyses of modern observatory data recording recent magnetic storms suggest that dayside field-aligned currents may have significantly affected disturbance at Colaba (e.g., Cid et al., 2015; Ohtani, 2022), and recent numerical simulations suggest that such field-aligned

Table 5. Hourly average storm intensities D^i, equation (5), calculated using the four standard observatories, Hermanus (HER), Kakioka (KAK), Honolulu (HON), and San Juan (SJG); local 1-min-resolution intensities, sampled as at Colaba, ${}_C d^i_n$, equation (12), for Alibag (ABG) and HER, KAK, HON, SJG for selected storms, 1989–2015. Month (Mn), Day (Dy), Hour (Hr, UT), Minute (Mi, UT). Bold data are shown in Figure 5.

Year	Mn	Dy	Hr	D^i (nT)	Mn	Dy	Hr	Mi	${}_C d^i_{ABG}$ (nT)	Mn	Dy	Hr	Mi	${}_C d^i_{HER}$ (nT)	Mn	Dy	Hr	Mi	${}_C d^i_{KAK}$ (nT)	Mn	Dy	Hr	Mi	${}_C d^i_{HON}$ (nT)	Mn	Dy	Hr	Mi	${}_C d^i_{SJG}$ (nT)
1989	03	14	01	**593**						03	14	01	37	663	03	14	01	37	**663**	03	14	00	27	**580**					
1991	11	09	01	**379**						11	08	22	42	356	11	09	00	42	**320**	11	09	02	27	357	11	09	00	47	448
1991	03	25	00	**295**						03	25	00	47	277	03	25	03	42	**315**	03	25	03	42	314	03	25	03	42	324
1990	04	10	15	**291**						04	10	16	32	340	04	10	14	52	337	04	10	15	27	200	04	10	18	17	**282**
1992	05	10	14	**284**						05	10	15	22	341	05	10	11	57	342	05	10	12	22	262	05	10	15	07	**288**
1991	10	29	08	279						10	28	15	52	239	10	28	15	47	276	10	29	07	27	251					
2003	11	20	20	**427**	11	20	19	12	690	11	20	21	07	433	11	20	19	52	468						11	20	19	12	**551**
2003	10	30	22	**384**	10	30	21	57	405	10	29	07	02	465	10	30	02	22	**363**	10	30	02	02	418	10	30	22	32	489
2001	03	31	08	**382**	03	31	08	12	**372**	03	31	19	12	332	03	31	08	37	407	03	31	08	07	459	03	31	20	52	325
2004	11	08	06	**371**	11	10	09	42	**385**	11	08	08	37	**395**	11	08	05	52	**437**	11	08	05	27	487	11	09	20	42	339
2000	07	16	00	**301**	07	15	21	57	385	07	15	22	12	337	07	16	01	42	**262**	07	15	20	57	**289**	07	15	22	32	374
2000	04	06	22	**297**	04	07	00	27	337	04	06	22	42	357	04	07	00	27	**298**	04	07	12	07	146	04	07	06	57	186
2015	03	17	22	**232**	03	17	16	42	273	03	17	16	57	252	03	17	17	32	185	03	17	23	47	**232**	03	17	23	17	295
2015	06	23	04	**195**	06	23	04	47	222	06	22	20	12	248	06	23	04	42	**223**	06	23	04	42	258	06	23	03	12	164
2015	12	20	22	**164**	12	20	18	22	190	12	20	18	47	192	12	21	00	02	**146**	12	21	02	37	168	12	20	22	47	209
2012	03	09	08	**141**	03	09	12	12	180	03	09	15	17	152	03	09	07	42	187	03	09	08	37	150	03	09	15	22	**111**
2012	07	15	16	141	07	15	16	12	176	07	15	18	27	184	07	15	09	02	158	07	15	09	07	142	07	15	21	47	166
2011	10	25	01	140	10	25	01	20	130	10	25	01	32	107	10	25	06	12	133	10	25	03	47	154	10	25	01	17	206

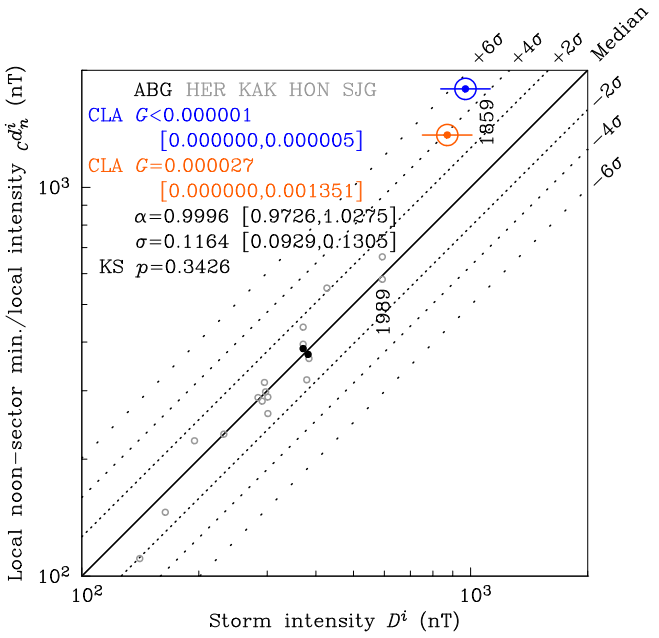

Figure 5. Contour lines of the (log)normal density function $g(\ln {}_C d^i_n | \ln D^i, \ln \alpha, \sigma)$, equation (13): median (black solid line) and $\pm 2\sigma$ intervals (dotted lines); intensities D^i and ${}_C d^i_n$ from Table 5 (1989–2015): Alibag (black, ABG) and the four standard *Dst* observatories (grey, open circles), Hermanus (HER), Kakioka (KAK), Honolulu (HON), San Juan (SJG). The model enables estimation of an exceedance probability $G(\ln {}_C d^i_n | \ln D^i, \ln \alpha, \sigma)$, equation (14), for a local-noon sector (09:00 to 14:59) intensity $\ln {}_C d^i_n$, equation (12) from a single low-latitude observatory, where data have been sparsely sampled as done at Colaba during the Carrington storm, given an hourly average storm intensity D^i, equation (5). G estimated with (blue) and without (orange) the extreme disturbance value at 06:20 UT.

currents might have resulted from unusually high solar-wind dynamic pressure and a dayside partial-ring current (e.g., Blake et al., 2021). Second, in circumstances like we have for the Carrington storm, with very unusual data originating from a single source, we should consider the possibility that there might be something wrong with the data. Indeed, Hayakawa et al. (2022a) call attention to the fact that the extreme local intensity value at 06:20 UT on September 2 is reported right after a hiatus or "gap" in the auxiliary measurements that were made during periods of unusual disturbance. As we note in Section 3, this gap is not explained in the Colaba yearbook. We wonder if the observatory workers were having difficulty obtaining accurate measurements during the extreme activity of the Carrington storm.

It is important to recognize that at least part of the seeming rarity of the extreme Colaba disturbance value at 06:20 UT is due to how the geomagnetic variation was sampled at Colaba – sparse spot sampling and only in the day sector. We examine modern 1-min-resolution observatory disturbance sequences from Alibag for 12 intense storms, years 2000–2015 (cycles 23–24). For each storm i, we obtain its hourly average intensity D^i. For local intensity, we examine every minute of each storm, regardless of local time

Table 6. Hourly average storm intensities D^i, equation (5), calculated using the four standard observatories, HER, KAK, HON, SJG; local 1-min-resolution intensities d^i_{ABG}, equation (15), for Alibag (ABG) for selected storms, 2000–2015. Month (Mn), Day (Dy), Hour (Hr, UT), Minute (Mi, UT). Data are shown in Figure 6.

Year	Mn	Dy	Hr	D^i (nT)	Mn	Dy	Hr	Mi	d^i_{ABG} (nT)
2003	11	20	20	427	11	20	19	12	690
2003	10	30	22	384	10	30	21	57	405
2001	03	31	08	382	03	31	08	12	372
2004	11	08	06	371	11	10	09	42	385
2000	07	16	00	301	07	15	21	57	385
2000	04	06	22	297	04	07	00	26	339
2015	03	17	22	232	03	17	16	42	273
2015	06	23	04	195	06	23	04	47	222
2015	12	20	22	164	12	20	18	22	190
2012	03	09	08	141	03	09	12	09	181
2012	07	15	16	141	07	15	16	13	176
2011	10	25	01	140	10	25	01	20	130

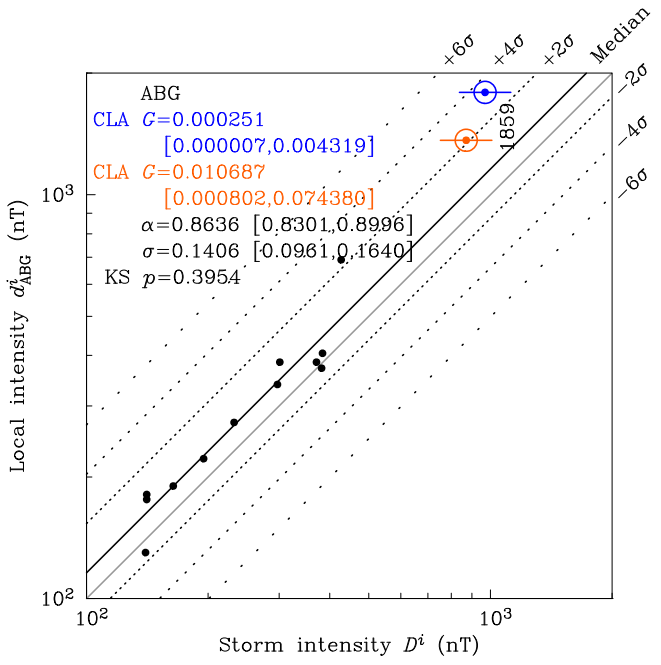

Figure 6. Contour lines of the (log)normal density function $g(\ln d^i_{\mathrm{ABG}} | \ln D^i, \ln \alpha, \sigma)$, equation (13): median (black solid line) and ±2σ intervals (dotted lines); intensities D^i and d^i_{ABG} from Table 6 (2000–2015): Alibag (black, ABG). G estimated with (blue) and without (orange) the extreme disturbance value at 06:20 UT.

$$d^i_{ABG} = \max_{t^i_j \in [t^i_s, t^i_e]} \left(-dist_{ABG}\left(t^i_j\right) \right); \qquad (15)$$

compare this with equations (7) and (12). In Table 6, we list D^i and d^i_{ABG} values, and in Figure 6, we plot these values and model fits. In the same figure, we plot the extreme hourly intensity, d^{1859}_{CLA} = 1821 nT, and storm intensity, D = 964 nT, corresponding to the inclusion of the extreme disturbance value at 06:20 UT, and the extreme auxiliary intensity, 1386 nT, and storm intensity, D = 866 nT, corresponding to exclusion of the extreme disturbance value at 06:20 UT. In comparison to the results shown in Figure 5, the small bias factor a = 0.8674 corresponds to a significant offset of median d^i_{ABG} compared to D^i – without the restrictions of subsampling, with more 1-min disturbance values from which to choose, local intensity values are higher than overall storm intensity. In this case, the probability that a storm with intensity D^{1859} = 964 nT would give rise to an hourly local intensity like the Colaba d^{1859}_{CLA} = 1821 nT value is very low, G = 0.000251. This is still rare, but, we emphasize, that the probabilities listed in Figure 5 are more meaningful because they are sampled like the Colaba data.

7 Conclusions

The uncertainty of the maximum –*Dst* of the Carrington storm is a primary factor affecting estimates of the occurrence frequency of extremely intense storms. So, for example, recalling results from Section 5, if one includes the extreme disturbance value at 06:20 UT in an hourly average of local-Colaba disturbance, then the median storm intensity of a storm giving rise to the observed disturbance at Colaba is D = 964 nT, with a 68% credibility interval of [855,1087] nT. Considering, then, the results of Love (2021), for a generalized extreme-value extrapolation of storms realized during solar cycles 14–24 (1902–2019), the most likely occurrence frequency of a storm with similar (or greater) intensity is 0.0107/solar cycle. For solar cycles with a typical duration of 10.73 years, this corresponds to a median wait time of 1003 years between such storms (also refer to Moriña et al., 2019). The 68% credibility interval is [0.0265,0.0038]/solar cycle, for a wait-time credibility interval of [405, 2824] years – an uncertainty in the occurrence frequency of almost a factor of seven due simply to the fact that the maximum –*Dst* of the Carrington storm is, itself, uncertain because it is inferred from observations made at a single observatory. If one were to prefer to exclude the extreme disturbance value at 06:20 UT because it might have been affected by non-ring currents or because it might be inaccurate, then one arrives at a median storm intensity of D = 866, [768, 977] nT. With generalized extreme-value extrapolation, the most likely occurrence frequency of storms with similar (or greater) intensity is 0.0241, [0.0536,0.0096]/solar cycle, for a median wait time of 445, [200, 1118] years. This is more than a factor of two shorter

than the case where we include the most extreme disturbance value.

At latitudes higher than Colaba, the interference that the Carrington storm brought to telegraph systems worldwide was plausibly due to geomagnetic disturbance generated by auroral-zone electrojet currents. Together with the storm's main-phase increase in *–Dst*, the auroral oval expanded in latitude, increasing the geographic area that experienced high levels of geomagnetic disturbance, and increasing the exposure of grounded telegraph systems to geoelectric fields induced in the Earth (e.g., Boteler, 2006b). Reports of overhead aurora down to about 25 magnetic latitude (e.g., Hayakawa et al., 2020a) suggest that telegraph systems across all of Europe, most of North America, Asia, and Australia, and large parts of South America and Africa, were exposed to interfering geoelectric fields. More recent, albeit less intense, storms caused power-grid system interference across North America coincident with an overhead auroral oval (e.g., Love et al., 2022). Assuming that what has occurred in the past will occur again in the future, the magnitudes of these events inform estimates of the exposure that would be realized for present-day power-grid systems due to a storm with an intensity comparable to the Carrington storm (e.g., Oughton et al., 2019; Ebihara et al., 2021).

Ironically, our modern, technologically-based society would be at greater risk if the intensity of the Carrington storm were actually relatively low. To understand this, consider the level of widespread disruption of long-line telegraph systems caused by the Carrington storm. A storm of comparable intensity might be expected to deliver a considerable level of disruption to grounded power-grid systems. But storms of relatively low intensity (small maximum *–Dst*) occur more frequently than storms with relatively high intensity (large maximum *–Dst*). Therefore, if the intensity of the Carrington storm were (say) on the low side of our estimated credibility intervals, then we would expect widespread disruption of technological systems to occur more frequently than if the intensity of the Carrington storm were, instead, on the high side of our estimated credibility intervals. And, insofar as risk is, in a statistical sense, proportional to the probability of the hazard in a given duration of time (e.g., Kron, 2002; Smolka, 2006), then the risk associated with a Carrington-class storm is higher if the intensity of the Carrington storm was on the lower end of our credibility interval. Overestimating the intensity of the Carrington storm, and underestimating the risk of a future Carrington-class storm, might result in under-mitigation for possible impacts. In such a scenario, the occurrence of a Carrington-class storm could cause widespread disruption of technological systems that have been left unprotected. That could be costly. On the other hand, underestimating the intensity of the Carrington storm, and overestimating the risk of a future Carrington-class storm, might motivate over-mitigation for possible impacts. In such a scenario, expensive protections installed on technological systems might not be necessary. Really, to properly prioritize mitigation projects, what is needed is an accurate estimate of the intensity of the Carrington storm. Unfortunately, that is exactly what we do not have.

Acknowledgements

We thank R. D. Gold, K. A. Lewis, B. R. Shiro, and J. M. Carter for proof-reading a draft manuscript. We thank A. Guerrero and M. A. Hapgood for journal reviews. This work was supported by the U.S. Geological Survey, Geomagnetism Program. The editor thanks Antonio Guerrero and Mike Hapgood for their assistance in evaluating this paper.

Data availability statement

The Colaba data for the Carrington storm presented by Hayakawa et al. (2022a) are available from https://www.kwasan.kyoto-u.ac.jp/~hayakawa/data/. Data for the September 1909 storm are available from Love et al. (2019b, their supporting information). Data for the May 1921 storm are available from Love et al. (2019a, their supporting information). Data for the October 1903, March 1940, and March 1946 storms are available from H. Hayakawa on request (hisashi@nagoya-u.jp). The Oulu *Dxt* index is available from the University of Oulu, Finland (dcx.oulu.fi). Historical observatory data are available from the Kyoto WDC at https://wdc.kugi.kyoto-u.ac.jp, from the Edinburgh WDC at https://wdc.bgs.ac.uk, and from INTERMAGNET at https://www.intermagnet.org.

References

Aitchison J, Brown JAC. 1957. *The lognormal distribution: With special reference to its uses in economics*. Cambridge University Press, Cambridge, UK. ISBN 978-0521040112.

Allen J, Sauer H, Frank L, Reiff P. 1989. Effects of the March 1989 solar activity. Eos Trans Am Geophys Union 70(46), 1479, 1486–1488. https://dx.doi.org/10.1029/89EO00409.

Asikainen T, Maliniemi V, Mursula K. 2010. Modeling the contributions of ring, tail, and magne-topause currents to the corrected Dst index. *J Geophys Res Space Phys* **115(A12)**: A12203. https://dx.doi.org/10.1029/2010JA015774.

Baker DN, Balstad R, Bodeau JM, Cameron E, Fennell JE, et al. 2008. *Severe space weather events – Understanding societal and economic impacts*. The National Academy Press, Washington, DC. ISBN 978-0-309-14153-6. https://dx.doi.org/10.17226/12507.

Beggan CD, Clarke E, Lawrence E, Eaton E, Williamson J, Matsumoto K, Hayakawa H. 2024. Digitized continuous magnetic recordings for the August/September 1859 storms From London, UK. *Space Weather* **22(3)**: e2023SW003, 807. https://doi.org/10.1029/2023SW003807.

Blake SP, Pulkkinen A, Schuck PW, Glocer A, Oliveira DM, Welling DT, Weigel RS, Quaresima G. 2021. Recreating the horizontal magnetic field at Colaba during the Carrington event with geospace simulations. *Space Weather* **19(5)**: e2020SW002, 585. https://dx.doi.org/10.1029/2020SW002585.

Boaghe OM, Balikhin MA, Billings SA, Alleyne H. 2001. Identification of nonlinear processes in the magnetospheric dynamics and forecasting of Dst index. *J Geophys Res Space Phys* **106(A12)**: 30047–30066. https://dx.doi.org/10.1029/2000JA900162.

Bohm G, Zech G. 2010. *Introduction to statistics and data analysis for physicists*. Verlag Deutsches Elektronen-Synchrotron, Hamburg, Germany. ISBN 978-3-935702-41-6.

Boteler DH. 2006a. Comment on time conventions in the recordings of 1859. *Adv Space Res* **38(2)**: 301–303. https://dx.doi.org/10.1016/j.asr.2006.07.006.

Boteler DH. 2006b. The super storms of August/September 1859 and their effects on the telegraph system. *Adv Space Res* **38(2)**: 159–172. https://dx.doi.org/10.1016/j.asr.2006.01.013.

Boteler DH. 2019. A 21st century view of the March 1989 magnetic storm. *Space Weather* **17(10)**: 1427–1441. https://dx.doi.org/10.1029/2019SW002278.

Box GEP, Tiao GC. 1992. *Bayesian inference in statistical analysis*. John Wiley & Sons, New York, NY. ISBN 9781118033197. https://dx.doi.org/10.1002/9781118033197.

Carrington RC. 1859. Description of a singular appearance seen in the Sun on September 1 1859. *Month Notices Royal Astron Soc* **20(1)**: 13–15. https://dx.doi.org/10.1093/mnras/20.1.13.

Chapman S, Bartels J. 1962. Geomagnetism, Volume 1. Oxford University Press, London, UK, 2 edn.

Cid C, Saiz E, Guerrero A, Palacios J, Cerrato Y. 2015. A Carrington-like geomagnetic storm observed in the 21st century. *J Space Weather Space Clim* **5**: A16. https://dx.doi.org/10.1051/swsc/2015017.

Clauset A, Shalizi CR, Newman MEJ. 2009. Power-law distributions in empirical data. *SIAM Rev* **51(4)**: 661–703. https://dx.doi.org/10.1137/070710111.

Cliver EW. 2006. The 1859 space weather event: Then and now. *Adv Space Res* **38(2)**: 119–129. https://dx.doi.org/10.1016/j.asr.2005.07.077.

Cliver EW, Dietrich WF. 2013. The 1859 space weather event revisited: Limits of extreme activity. *J Space Weather Space Clim* **3**: A31. https://dx.doi.org/10.1051/swsc/2013053.

Cliver EW, Svalgaard L. 2005. The 1859 solar-terrestrial disturbance and the current limits on extreme space weather activity. *Solar Phys* **224**: 407–422. https://dx.doi.org/10.1007/s11207-005-4980-z.

Corral Á, González A. 2019. Power law size distributions in geoscience revisited. *Earth Space Sci* **6(5)**: 673–697. https://dx.doi.org/10.1029/2018EA000479.

Crow EL, Shimizu K, (Eds.). 1988. *Lognormal distributions: theory and applications*. Marcel Dekker, New York, NY. ISBN 9780824778033.

Daglis IA, (Ed.). 2005. *Effects of space weather on technology infrastructure*. Springer, Dordrecht, The Netherlands. ISBN 978-1-4020-2754-3. https://dx.doi.org/10.1007/1-4020-2754-0.

Daglis IA. 2006. Ring current dynamics. *Space Sci Rev* **124(1–4)**: 183–202. https://dx.doi.org/10.1007/s11214-006-9104-z.

Dessler AJ, Parker EN. 1959. Hydromagnetic theory of geomagnetic storms. *J Geophys Res* **64(12)**: 2239–2252. https://dx.doi.org/10.1029/JZ064i012p02239.

Eastwood JP, Biffis E, Hapgood MA, Green L, Bisi MM, Bentley RD, Wicks R, McKinnell L-A, Gibbs M, Burnett C. 2017. The economic impact of space weather: Where do we stand?. *Risk Anal* **37(2)**: 206–218. https://dx.doi.org/10.1111/risa.12765.

Ebihara Y, Watari S, Kumar S. 2021. Prediction of geomagnetically induced currents (GICs) flowing in Japanese power grid for Carrington-class magnetic storms. *Earth Planets Space* **73**. https://dx.doi.org/10.1186/s40623-021-01493-2.

Efron B, Tibshirani RJ. 1994. *An introduction to the bootstrap*. Chapman and Hall/CRC, New York, NY. https://doi.org/10.1201/9780429246593.

Fergusson EFT. 1860. *Magnetical and meteorological observations made at the government observatory, Bombay, 1859*. Bombay Education Society's Press, Byculla, India.

Friedrich E, Rostoker G, Connors MG, McPherron RL. 1999. Influence of the substorm current wedge on the Dst index. *J Geophys Res Space Phys* **104(A3)**: 4567–4575. https://dx.doi.org/10.1029/1998JA900096.

Gannon JL, Love JJ. 2011. USGS 1-min *Dst* index. *J Atmos Solar-Terrestrial Phys* **73(2)**: 323–334. https://dx.doi.org/10.1016/j.jastp.2010.02.013.

Gawali PB, Doiphode MG, Nimje RN. 2015. Colaba-Alibag magnetic observatory and Nanabhoy Moos: The influence of one over the other. *History Geo Space Sci* **6(2)**: 107–131. https://dx.doi.org/10.5194/hgss-6-107-2015.

Gjerloev JW. 2009. A global ground-based magnetometer initiative. *Eos Trans Am Geophys Union* **90(27)**: 230–231. https://dx.doi.org/10.1029/2009EO270002.

Gonzalez WD, Echer E, Tsurutani BT, Clúa de González AL, Dal Lago A. 2011. Interplanetary origin of intense, superintensive and extreme geomagnetic storms. *Space Sci Rev* **158(1)**: 69–89. https://dx.doi.org/10.1007/s11214-010-9715-2.

Gonzalez WD, Joselyn JA, Kamide Y, Kroehl HW, Rostoker G, Tsurutani BT, Vasyliunas VM. 1994. What is a geomagnetic storm?. *J Geophys Res* **99(A4)**: 5771–5792. https://dx.doi.org/10.1029/93JA02867.

Green JL, Boardsen S, Odenwald S, Humble J, Pazamickas KA. 2006. Eyewitness reports of the great auroral storm of 1859. *Adv Space Res* **39(2)**: 145–154. https://dx.doi.org/10.1016/j.asr.2005.12.021.

Hapgood M. 2019. The great storm of May 1921: An exemplar of a dangerous space weather event. *Space Weather* **17(7)**: 950–975. https://dx.doi.org/10.1029/2019SW002195.

Hapgood MA. 2012. Prepare for the coming space weather storm. *Nature* **484**: 311–313. https://dx.doi.org/10.1038/484311a.

Hayakawa H, Ebihara JRRY, Correia AP, Sôma M. 2020a. South American auroral reports during the Carrington storm. *Earth Planets Space* **72(1)**: 122. https://dx.doi.org/10.1186/s40623-020-01249-4.

Hayakawa H, Ebihara Y, Cliver EW, Hattori K, Toriumi S, et al. 2019. The extreme space weather event in September 1909. *Month Notices Royal Astron Soc* **484(3)**: 4083–4099. https://dx.doi.org/10.1093/mnras/sty3196.

Hayakawa H, Ebihara Y, Hand DP, Hayakawa S, Kumar S, Mukherjee S, Veenadhari B. 2018. Low-latitude aurorae during the extreme space weather events in 1859. *Astrophys J* **869(1)**: 57. https://dx.doi.org/10.3847/1538-4357/aae47c.

Hayakawa H, Ebihara Y, Pevtsov AA, Bhaskar A, Karachik N, Oliveira DM. 2020b. Intensity and time series of extreme solar-terrestrial storm in 1946 March. *Month Notices Royal Astron Soc* **497(4)**: 5507–5517. https://dx.doi.org/10.1093/mnras/staa1508.

Hayakawa H, Nevanlinna H, Blake SP, Ebihara Y, Bhaskar AT, Miyoshi Y. 2022a. Temporal variations of the three geomagnetic field components at Colaba Observatory around the Carrington storm in 1859. *Astrophys J* **928(1)**: 32. https://dx.doi.org/10.3847/1538-4357/ac2601.

Hayakawa H, Oliveira DM, Shea MA, Smart DF, Blake SP, Hattori K, Bhaskar AT, Curto JJ, Franco DR, Ebihara Y. 2022b. The extreme solar and geomagnetic storms on 1940 March 20–25. *Month Notices Royal Astron Soc* **517(2)**: 1709–1723. https://dx.doi.org/10.1093/mnras/stab3615.

Hayakawa H, Ribeiro P, Vaquero JM, Knipp MCGDJ, Mekhaldi F, et al. 2020c. The extreme space weather event in 1903 October/November: An outburst from the quiet Sun. *Astrophys J Lett* **897(1)**: L10. https://dx.doi.org/10.3847/2041-8213/ab6a18.

Hodgson R. 1859. On a curious appearance seen in the Sun. *Month Notices Royal Astron Soc* **20(1)**: 15–16. https://dx.doi.org/10.1093/mnras/20.1.15a.

Hudson HS. 2021. Carrington events. *Annu. Rev Astron Astrophys* **59(1)**: 445–477. https://dx.doi.org/10.1146/annurev-astro-112420-023324.

Ishii M, Shiota D, Tao C, Ebihara Y, Fujiwara H, et al. 2021. Space weather benchmarks on Japanese society. *Earth Planets Space* **73(1)**: 108. https://dx.doi.org/10.1186/s40623-021-01420-5.

Iyemori T, Takeda M, Nosé M, Odagi Y, Toh H. 2010. *Mid-latitude geomagnetic indices ASY and SYM for 2009 (Provisional). Internal report of data analysis center for geomagnetism and space magnetism*. Kyoto University, Japan. https://wdc.kugi.kyoto-u.ac.jp/aeasy/asy.pdf.

Jeffreys H. 1961. *Theory of probability*. Clarendon Press, Oxford, UK. ISBN 9780198503682, 0198503687.

Jones HS. 1955. *Sunspots and geomagnetic-storm data derived from Greenwich observations, 1874-1954*. Her Majesty's Stationery Office, London, UK.

Karinen A, Mursula K. 2005. A new reconstruction of the Dst index for 1932–2002. *Ann Geophys* **23(2)**: 475–485. https://dx.doi.org/10.5194/angeo-23-475-2005.

Koenig C, Liu H, Schoot RVD, Depaoli S, eds. 2022. Moving beyond non-informative prior distributions: achieving the full potential of Bayesian methods for psychological research. Frontiers Media SA. ISBN 9782889742141, 2889742148.

Kotzé P. 2018. Hermanus magnetic observatory: A historical perspective of geomagnetism in southern Africa. *History Geo-Space Sci* **9(2)**: 125–131. https://dx.doi.org/10.5194/hgss-9-125-2018.

Kron W. 2002. Keynote lecture: Flood risk = hazard × exposure × vulnerability. In: *Flood Defence '2002*, vol **1**, Wu B, Wang ZY, Wang GQ, Huang GH, Fang HW, Huang JC, (Eds.) Science Press, New York, NY. pp. 82–97. ISBN 978-1880132548.

Lakhina GS, Tsurutani BT. 2018. Super geomagnetic storms: Past, present and future. In: *Extreme space weather: Origins, predictability, and consequences, chap. 7*, Buzulukova N, (Ed.) Elsevier, Amsterdam, The Netherlands. pp. 157–185. ISBN 978-0-12-812700-1. https://doi.org/10.1016/C2016-0-03769-5.

Lewontin RC. 1966. On the measurement of relative variability. *Syst Zool* **15(2)**: 141–142. https://dx.doi.org/10.2307/sysbio/15.2.141.

Loewe CA, Prölss GW. 1997. Classification and mean behavior of magnetic storms. *J Geophys Res* **102(A7)**: 14209–14213. https://dx.doi.org/10.1029/96JA04020.

Love JJ. 2009. Missing data and the accuracy of magnetic-observatory hour means. *Ann Geophys* **27(9)**: 3601–3610. https://www.ann-geophys.net/27/3601/2009/.

Love JJ. 2021. Extreme-event magnetic storm probabilities derived from rank statistics of historical Dst intensities for solar cycles 14–24. *Space Weather* **19(4)**: e2020SW002, 579. https://dx.doi.org/10.1029/2020SW002579.

Love JJ, Finn CA. 2011. The USGS Geomagnetism Program and its role in space weather monitoring. *Space Weather* **9(7)**: S07001. https://dx.doi.org/10.1029/2011SW000684.

Love JJ, Gannon JL. 2009. Revised Dst and the epicycles of magnetic disturbance: 1958–2007. *Ann Geophys* **27(8)**: 3101–3131. https://doi.org/10.5194/angeo-27-3101-2009.

Love JJ, Hayakawa H, Cliver EW. 2019a. Intensity and impact of the New York Railroad superstorm of May 1921. *Space Weather* **17(8)**: 1281–1292. https://dx.doi.org/10.1029/2019SW002250.

Love JJ, Hayakawa H, Cliver EW. 2019b. On the intensity of the magnetic superstorm of September 1909. *Space Weather* **17(1)**: 37–45. https://dx.doi.org/10.1029/2018SW002079.

Love JJ, Lucas GM, Rigler EJ, Murphy BS, Kelbert A, Bedrosian PA. 2022. Mapping a magnetic superstorm: March 1989 geoelectric hazards and impacts on the United States power systems. *Space Weather* **20(5)**: e2021SW003, 030. https://dx.doi.org/10.1029/2021SW003030.

Love JJ, Tsai VC, Gannon JL. 2010. Averaging and sampling for magnetic-observatory hourly data. *Ann Geophys* **28(11)**: 2079–2096. https://dx.doi.org/10.5194/angeo-28-2079-2010.

Matta CF, Massa L, Gubskaya AV, Knoll E. 2011. Can one take the logarithm or the sine of a dimensioned quantity or a unit? Dimensional analysis involving transcendental functions. *J Chem Educ* **88(1)**: 67–70. https://dx.doi.org/10.1021/ed1000476.

Minamoto Y. 2013. Availability and access to data from Kakioka Magnetic Observatory, Japan. *Data Sci J* **12**: G30–G35. https://dx.doi.org/10.2481/dsj.G-040.

Moos NAF. 1910. *Colaba magnetic data, 1846 to 1905. Part I: Magnetic data and instruments*. Government Central Press, Bombay, India.

Moriña D, Serra I, Puig P, Corral Á. 2019. Probability estimation of a Carrington-like geomagnetic storm. *Sci Rep* **9(1)**: 2393. https://dx.doi.org/10.1038/s41598-019-38918-8.

Mursula K, Holappa L, Karinen A. 2008. Correct normalization of the *Dst* index. *Astrophys Space Sci Trans* **4(2)**: 41–45. https://dx.doi.org/10.5194/astra-4-41-2008.

Mursula K, Holappa L, Karinen A. 2011. Uneven weighting of stations in the Dst index. *J Atmos Solar-Terrestrial Phys* **73(2)**: 316–322. https://doi.org/10.1016/j.jastp.2010.04.007.

O'Hagan A, Forster J. 2004. Kendall's advanced theory of statistics. In: *Bayesian Inference*, 2nd edn, vol **2B**, Arnold, London, UK. ISBN 978-0-470-68569-3.

Ohtani S. 2022. New insights from the 2003 Halloween Storm into the Colaba 1600 nT magnetic depression during the 1859 Carrington storm. *J Geophys Res Space Phys* **127(9)**: e2022JA030, 596. https://dx.doi.org/10.1029/2022JA030596.

Ohtani S, Nosé M, Rostoker G, Singer H, Lui ATY, Nakamura M. 2001. Storm-substorm relationship: Contribution of the tail current to Dst. *J Geophys Res Space Phys* **106(A10)**: 21199–21209. https://dx.doi.org/10.1029/2000JA000400.

Olea RA, Pawlowsky-Glahn V. 2009. Kolmogorov-Smirnov test for spatially correlated data. *Stoch Environ Res Risk Assess* **23(6)**: 749–757. https://dx.doi.org/10.1007/s00477-008-0255-1.

Oughton EJ, Hapgood M, Richardson GS, Beggan CD, Thomson AWP, et al. 2019. A risk assessment framework for the socio-economic impacts of electricity transmission infrastructure failure due to space weather. *Risk Anal* **39(5)**: 1022–1043. https://dx.doi.org/10.1111/risa.13229.

Piccinelli R, Krausmann E. 2014. *Space weather and power grids – A vulnerability assessment*. European Union, Luxembourg. ISBN 978-92-79-43971-1. https://dx.doi.org/10.2788/20848.

Press WH, Teukolsky SA, Vetterling WT, Flannery BP. 1992. *Numerical Recipes in Fortran 77*, 2nd edn. Cambridge University Press, Cambridge, UK. ISBN 978-0521430647.

Rigler EJ. 2017. Time-causal decomposition of geomagnetic time series into secular variation, solar quiet, and disturbance signals. U.S. Geological Survey Open-File Report, 2017–1037. https://dx.doi.org/10.3133/ofr20171037.

Roe BP. 2001. *Probability and statistics in experimental physics. Undergraduate texts in contemporary physics*. Springer-Verlag, New York, NY. ISBN 978-1-4684-9296-5. https://dx.doi.org/10.1007/978-1-4684-9296-5.

Saiz E, Cid C, Guerrero A. 2021. The relevance of local magnetic records when using extreme space weather events as benchmarks. *J Space Weather Space Clim* **11**: 35. https://doi.org/10.1051/swsc/2021018.

Sckopke N. 1966. A general relation between the energy of trapped particles and the disturbance field over the Earth. *J Geophys Res* **71(13)**: 3125–3130. https://dx.doi.org/10.1029/JZ071i013p03125.

Silverman SM. 2006. Comparison of the aurora of September 1/2 1859 with other great auroras. *Adv Space Res* **38(2)**: 136–144. https://dx.doi.org/10.1016/j.asr.2005.03.157.

Siscoe GL, Crooker NU, Clauer CR. 2006. *Dst* of the Carrington storm of 1859. *Adv Space Res* **38(2)**: 173–179. https://dx.doi.org/10.1016/j.asr.2005.02.102.

Smolka A. 2006. Natural disasters and the challenge of extreme events: Risk management from an insurance perspective. *Philos Trans Royal Soc London Ser A* **364**: 2147–2165. https://dx.doi.org/10.1098/rsta.2006.1818.

Steinskog DJ, Thøstheim DB, Kvamstø NG. 2007. A cautionary note on the use of the Kolmogorov-Smirnov test for normality. *Month Weather Rev* **135(3)**: 1151–1157. https://dx.doi.org/10.1175/MWR3326.1.

Sugiura M. 1964. Hourly values of equatorial *Dst* for the IGY. *Ann Int Geophys Year* **35**: 9–45.

Sugiura M, Kamei T. 1991. Equatorial Dst index 1957–1986. IAGA Bulletin, 40, International Service of Geomagnetic Indices Publication Office, Saint-Maur-des-Fossess, France.

Tsubouchi K, Omura Y. 2007. Long-term occurrence probabilities of intense geomagnetic storm events. *Space Weather* **5(12)**. https://dx.doi.org/10.1029/2007SW000329.

Tsurutani BT, Gonzalez WD, Lakhina GS, Alex S. 2003. The extreme magnetic storm of 1–2 September 1859. *J Geophys Res* **108(A7)**. https://dx.doi.org/10.1029/2002JA009504.

Turner NE, Baker DN, Pulkkinen TI, McPherron RL. 2000. Evaluation of the tail current contribution to Dst. *J Geophys Res* **105(A3)**: 5431–5439. https://dx.doi.org/10.1029/1999JA000248.

Usoskin I, Miyake F, Baroni M, Brehm N, Dalla S, et al. 2023. Extreme solar events: Setting up a paradigm. *Space Sci Rev* **219(8)**: 73. https://dx.doi.org/10.1007/s11214-023-01018-1.

Vassiliadis D, Klimas AJ, Valdivia JA, Baker DN. 2000. The nonlinear dynamics of space weather. *Adv Space Res* **26(1)**: 197–207. https://doi.org/10.1016/S0273-1177(99)01050-9.

von Storch H. 1995. Misuses of statistical analysis in climate research. In: *Analysis of climate variability: Applications and Statistical techniques*. von Storch H, Navarra A, (Eds.) Springer-Verlag, New York, NY. pp. 11–25. ISBN 978-3-662-03169-8.

Wilks DS. 2006. *Statistical methods in the atmospheric sciences*. Elsevier, Amsterdam, The Netherlands ISBN 978-0-12-751966-1.

Appendix

We summarize some relevant statistical properties of the normal and lognormal distributions.

The lognormal distribution

By the central limit theorem of statistics, a population of random variables y generated from the addition of a large number of random and independent sub-variables, drawn from well-behaved but not necessarily identical distributions will be normally distributed and have the probability density

$$g(y|\mu,\sigma) = \frac{1}{\sigma\sqrt{2\pi}} \exp\left[-\frac{(y-\mu^2)}{2\sigma^2}\right], \quad \text{(A1)}$$

where the parameters μ and σ are the mean and standard deviation, respectively, of the y variables. By simple corollary, if a population of positive random variables x is generated from the multiplication of a large number of positive, random, and independent sub-variables, drawn from well-behaved but not necessarily identical distributions then the variables Inx will be normally distributed with density

$$g(\ln x|\mu,\sigma) = \frac{1}{\sigma\sqrt{2\pi}} \exp\left[-\frac{(\ln x-\mu^2)}{2\sigma^2}\right], \quad \text{(A2)}$$

where, now, μ and σ are the mean and standard deviation, respectively, of the Inx variables (not of the x variables). By the chain rule of differentiation,

$$g(\ln x)d\ln x = d(\ln x)\frac{d\ln x}{dx}dx = g(\ln x)\frac{dx}{x} = \lambda(x)dx, \quad \text{(A3)}$$

where the probability density function for a lognormally distributed variable x is

$$\lambda(x|\mu,\sigma) = \frac{1}{x\sigma\sqrt{2\pi}} \exp\left[-\frac{(\ln x-\mu)^2}{2\sigma^2}\right] \quad \text{(A4)}$$

(e.g., Aitchison and Brown, 1957; Crow and Shimizu, 1988). Even if the variables x have physical units, their logarithms are conventionally considered to be dimensionless (e.g., Matta et al., 2011).

Bayesian symmetry

Important insight concerning the normal distribution can be obtained from a simple interpretation of Bayesian probability, under which model parameters are assumed to be random variables that are related to the distribution of data (e.g., O'Hagan and Forster, 2004). We write Bayes's equation,

$$g(y|\mu,\sigma)\cdot p(\mu) = g(\mu|y,\sigma)\cdot p(y). \quad \text{(A5)}$$

Here, $g(y|\mu, \sigma)$ is interpreted as the conditional probability density of the variable y, given an occurrence in the probability of the mean μ (we are interpreting σ to be a nonprobabilistic parameter). Conversely, $g(y|\mu, \sigma)$ is interpreted as the conditional "posterior" probability density of μ, given the probability of an instance of y (and the parameter σ). $p(\mu)$ is the (unconditional) "prior" probability density of μ. Typically, in working with Bayes's equation, one uses the prior to summarize one's preexisting knowledge or subjective prejudice concerning the parameter of interest. It is not our intent, here, to delve into the difficult philosophy that sometimes accompanies the choice of a prior, especially "informative" priors that significantly affect inference (e.g., Koenig et al., 2022). Seeking simplicity, we choose the "uninformative" prior suggested by Jeffreys (1961). This ensures that any inference is independent of the way the probability functions are parameterized. The Jeffreys prior for the mean of a normal distribution is just the unnormalized uniform distribution; in our case,

$$p(\mu) = 1. \quad \text{(A6)}$$

In contrast, $p(y)$, the "posterior" probability density of y, plays a passive role, one that ensures that equation (A5) is properly normalized. In our case,

$$p(y) = 1. \quad \text{(A7)}$$

With these choices, we obtain,

$$g(y|\mu,\sigma) = g(\mu|y,\sigma). \quad \text{(A8)}$$

This simple-looking equation represents more than just a mathematical symmetry, it carries important interpretation: the parameter μ is normally distributed if the data y are normally distributed, and the two have identical standard deviations σ (e.g., Box and Tiao, 1992, their Section 1.3.1). If the variables ln x are normally distributed, then

$$g(\ln x|\mu,\sigma) = g(\mu|\ln x,\sigma). \tag{A9}$$

Scale invariance

Let us now consider a population of positive variables z (not necessarily normally or lognormally distributed). We can scale these variables by a positive factor θ and take their logarithms,

$$\ln(z\cdot\theta) = \ln z + \ln\theta. \tag{A10}$$

The effect of such a scaling on the mean of the logarithms of the variables is straightforward; it is shifted,

$$\begin{aligned}\mathrm{mean}\{\ln(z\cdot\theta)\} &= \mathrm{mean}\{\ln z\} + \mathrm{mean}\{\ln\theta\}\\ &= \mathrm{mean}\{\ln z\} + \ln\theta.\end{aligned} \tag{A11}$$

But the variance is unaffected by the same scaling,

$$\mathrm{var}\{\ln(z\cdot\theta)\} = \mathrm{var}\{\ln z\} + \mathrm{var}\{\ln\theta\} = \mathrm{var}\{\ln z\}. \tag{A12}$$

Because the variance of a constant is zero. Correspondingly,

$$\mathrm{sd}\{\ln(z\cdot\theta)\} = \mathrm{sd}\{\ln z\}. \tag{A13}$$

One can say that the variance (and the standard deviation) of the logarithms of the variables is scale-invariant (Lewontin, 1966). With this, we understand that equation (A2) has the property of scale-invariance,

$$g(\ln(x\cdot\theta)|\mu,\sigma) = g(\ln x|\mu+\ln\theta,\sigma). \tag{A14}$$

Cite this article as: Love JJ, Joshua Rigler E, Hayakawa H & Mursula K. 2024. On the uncertain intensity estimate of the 1859 Carrington storm. *J. Space Weather Space Clim.* **14**, 21. https://doi.org/10.1051/swsc/2024015.